MNRAS **000**, 1–11 (2011) Preprint 14 January 2019 Compiled using MNRAS LaTeX style file v3.0

Rotational modulation in *TESS* B stars

L. A. Balona[1], G. Handler[2], S. Chowdhury[2], D. Ozuyar[3], C. A. Engelbrecht[4], G. M. Mirouh[5], G. A. Wade[6], A. David-Uraz[7]
[1] *South African Astronomical Observatory, P.O. Box 9, Observatory, Cape Town 4735, South Africa*
[2] *Nicolaus Copernicus Astronomical Center, Bartycka 18, PL-00-716 Warsaw, Poland*
[3] *Department of Astronomy and Space Science, Ankara University, 06100 Tandogan-Ankara, Turkey*
[4] *Department of Physics, University of Johannesburg, PO Box 524, Auckland Park, Johannesburg, South Africa*
[5] *Astrophysics Research Group, Faculty of Engineering and Physical Sciences, University of Surrey, Guildford GU2 7XH, UK*
[6] *Department of Physics & Space Science, Royal Military College of Canada, P.O. Box 17000, Station Forces, Kingston, Ontario, Canada, K7K 7B4*
[7] *Department of Physics and Astronomy, University of Delaware, Newark, DE 19716, USA*

Accepted .... Received ...

ABSTRACT

Light curves and periodograms of 160 B stars observed by the *TESS* space mission and 30 main-sequence B stars from *Kepler* and *K2* were used to classify the variability type. Out of the 114 main-sequence B stars observed by *TESS*, 45 were classified as rotational variables. *Gaia* DR2 parallaxes were used to estimate luminosities, from which the radii and equatorial rotational velocities can be deduced. The relationship between projected rotational velocity and the equatorial rotational velocity is consistent with rotational modulation. We conclude that a large fraction of B stars appear to contain surface features which cannot likely be attributed to abundance patches.

Key words: stars: early-type - stars:rotation - stars: starspots - stars:oscillations

1 INTRODUCTION

The existence of large spots or spot groups on the surfaces of cool stars other than the Sun is well established. This discovery can be traced back to Kron (1947) who observed four eclipsing binaries and detected significant light variability outside eclipse that could not be explained other than by the presence of spots similar to those on the Sun. These stars were later called RS CVn binaries. Hall (1972) was the first to explicitly postulate the starspot model in these stars. Rotational modulation due to starspots is also detected in the BY Dra variables, which are emission-line K and M dwarfs, and in the FK Com stars, which are rapidly rotating G-K giants with emission in the CaII lines. Over 500 field stars showing evidence of starspots are known (see Strassmeier 2009 for a review), but many thousands have been detected from the *Kepler* space mission (McQuillan et al. 2013, 2014; Reinhold et al. 2013; Nielsen et al. 2013; Chowdhury et al. 2018).

Sunspots appear cooler than the surrounding photosphere because they correspond to regions of lower convective energy transport. The decrease in energy transport is due to strong localized magnetic fields which affect the convective motions close to the stellar surface. The magnetic fields are thought to be a result of dynamo action in the convective outer envelope of the Sun and other cool stars (Charbonneau 2014). From this perspective, only stars with outer convective envelopes can support such a magnetic field. Hence dark starspots are not expected in A and B stars which have radiative envelopes.

The chemically peculiar Ap and Bp stars do, however, show rotational light modulation due to patches of differing chemical abundances on the stellar surface. The chemical peculiarities are believed to be confined to the outer layers of the star and are generally thought to be a result of gravitational settling and diffusion of elements in the presence of a strong global magnetic field (Michaud 1970). For these stars, which have radiative atmospheres, the magnetic field is thought to be of fossil origin.

The discovery that a large fraction of A and B stars observed by *Kepler* seem to show rotational modulation (Balona 2013, 2016, 2017) and some of them possibly even flares (Balona 2012) was therefore unexpected. The possible existence of rotational modulation among the B stars suggests that our current understanding of the physics of the outer layers of hot stars may need to be revised. The fact that a great majority of δ Scuti stars show unexpected low frequencies (Balona 2018), which cannot be explained by current models, also points to such a revision.

The Transiting Exoplanet Survey Satellite mission (*TESS*; Ricker et al. 2015) is designed to search for exoplanets. A preliminary report on B stars from the first set of observations (Sectors 1 and 2) covering 55 d can be found in Pedersen et al. (2019). Our main aim is to classify the *TESS* B stars observed in Sectors 1 and 2 into various variability types, to estimate the approximate fraction of main sequence stars which might be rotational variables and to determine if the photometric periods are consistent with the presumed rotational periods.

2 DATA AND ANALYSIS

The *TESS* survey divides the sky into 26 partially overlapping sectors, each of which is observed for approximately one month during the two-year primary mission. The data analyzed in this paper are from the light curves of the first release (Sector 1 and Sector 2). A description of how these data products were generated is found in Jenkins et al. (2016). Sector 1 and Sector 2 observations each comprise a time span of about 27.5 d, with most stars observed over the full 55-d time interval.

Light curves are generated with two-minute cadence using simple aperture photometry (SAP) and pre-search data conditioning (PDC). The PDC pipeline module uses singular value decomposition to identify and correct for time-correlated instrumental signatures in the light curves. In addition, PDC corrects the flux for each target to account for crowding from other stars and their effects. Only PDC light curves are used in this paper. The combined differential photometric precision at 1-hour timescales for a 10-th magnitude star is about 230 ppm.

The *TESS* input catalogue (Stassun et al. 2018) lists stellar parameters for stars observed by *TESS*. The effective temperatures, $T_{\rm eff}$, for stars without spectroscopic determinations were obtained from near-infrared photometry, which is not reliable for B stars, particularly since reddening is important in most of these stars. For this reason B stars in Sectors 1 and 2 were selected from the SIMBAD astronomical database (Wenger et al. 2000), giving a total of 160 stars with spectral types earlier than A0.

Periodograms and light curves were visually inspected and each star assigned a variability class where appropriate. A necessary signature of rotational modulation is taken to be a significant, isolated low-amplitude peak with frequency less than 4 $\rm d^{-1}$ or a low-amplitude peak with one or more harmonics. The classification was made independently by LAB and GH with agreement among the stars deemed to be rotational variables.

3 ROTATIONAL VARIABILITY

The equatorial rotational velocity, v_e ($\rm km\,s^{-1}$), is given by $v_e = 50.74\nu_{\rm rot}(R/R_\odot)$, where the rotational frequency, $\nu_{\rm rot}$ is in cycles $\rm d^{-1}$ and $R/R_\odot$ is the stellar radius in solar units. For main-sequence B stars the radii are typically 2–10 $R/R_\odot$ and v_e in the range 0–400 $\rm km\,s^{-1}$. Thus one might expect $0 < \nu_{\rm rot} < 4\,\rm d^{-1}$. A periodogram peak in this frequency range could be a result of rotational modulation.

There are two ways to show that the variability of a group of stars might be due to rotational modulation. One way is to demonstrate that there is a relationship between the projected rotational velocities, $v\sin i$, and the equatorial rotational velocities, v_e. Since $\sin i \leq 1$, the expectation is that in a plot of $v\sin i$ as a function of v_e, the points will all lie on or below the line $v\sin i = v_e$, subject to measurement errors (see Fig. 2 in Balona 2017).

Another method is to show that, for stars in the main sequence band, the distribution of v_e, derived from $\nu_{\rm rot}$ and an estimate of the stellar radii, matches the distribution of v_e derived from spectroscopic measurements of $v\sin i$ for stars in the general field within the same temperature range (see Fig. 8 in Balona 2013). This has the advantage that values of $v\sin i$ of the stars to be tested are not required. A sufficient number of stars in each v_e bin is necessary and the number of bins needs to be sufficiently large to adequately resolve the distribution. The method therefore requires a rather large number of stars. The number of B stars with photometrically derived rotation periods is, at present, too few for this method to be applied.

Classification of stars according to variability type is an essential first step in any analysis. The information at hand is very limited: the light curve, the periodogram and the approximate location of the star in the H-R diagram as judged by the spectral type and the *Gaia* DR2 parallax.

It is reasonable to adopt the variability type definitions in the *General Catalogue of Variable Stars* (GCVS, Samus et al. 2009). There may be variability which does not seem to fit in any of the GCVS classes. Unless there is additional supporting evidence, the temptation must be resisted to assign a new class of variable. Since the GCVS does not include a type for rotational variables among the A and B stars, we have chosen ROT as a suitable designation for any star exhibiting rotational modulation, but not known to be chemically peculiar.

The SXARI variables are a specific set of B0p-B9p rotational variables with variable-intensity HeI and SiIII lines and magnetic fields. The periods of their light and magnetic field variations are consistent with rotation. They are high-temperature analogs of the α^2 CVn (ACV) variables, which are Ap stars with a tilted global magnetic field and abundance patches, giving rise to rotational modulation of the light curve. If a star shows signs of abnormalities, such as enhanced Si, Mg or Hg or is He weak or He strong, then the variability is likely a result of a patch or patches of enhanced chemical abundance. The star should then be classified as SXARI rather than ROT in accordance with the GCVS system. The photometric frequency is, however, still the rotational frequency just as it is in the ROT type.

Binaries in a circular orbit may give rise to a low frequency peak either through tidal effects (ELL type of variable) or grazing eclipses. Eclipses are easy to spot as they give rise to a large number of harmonics in the periodogram. Tidal effects cannot easily be distinguished from rotational modulation. The ambiguity between the ELL and ROT classifications can be broken if there is significant amplitude or frequency modulation.

4 OTHER TYPES OF VARIABILITY IN B STARS

There are two main types of pulsating variable among the B stars, the β Cep (called BCEP in the GCVS) and “slowly pulsating B-star” (SPB) variables. The pulsations in both

Table 1. List of B stars observed by *TESS*. The TIC number and the star name is given in the first two columns. This is followed by the assigned variability type and the apparent V magnitude. $\nu_{\rm rot}$ is the presumed rotational frequency and v_e is the equatorial rotational velocity derived from $\nu_{\rm rot}$. The projected rotational velocity, $v \sin i$, is from spectroscopic measurements in the literature. The adopted effective temperature, $T_{\rm eff}$, and the stellar luminosity obtained from the *Gaia* parallax are shown. The spectral type is given in the last column ("(Be)" indicates a classical Be star).

TIC	Name	Var. Type	V mag	$\nu_{\rm rot}$ (d^{-1})	v_e (km/s)	$v \sin i$ (km/s)	$T_{\rm eff}$ (K)	$\log \frac{L}{L_\odot}$	Sp. Type
12359289	HD 225119	SXARI	8.180	0.325	65		15330	2.90	kB8hB7HeB9.5IIISi
29990592	HD 268623	ACYG	11.635				20665		B1.5Ia (LMC)
30110048	HD 268653	ACYG	10.760				17185		B2.5Ia (LMC)
30268695	HD 268809	ACYG	11.964				22845		B0.5Ia (LMC)
30275662	Sk-66 27	ACYG	11.779				17765		B2.5/3Ia (LMC)
30312676	HD 268726	ACYG	11.265				19075		B2Iaq (LMC)
30317301	HD 268798	EB	11.490				28000		B0.5, B2Ia (LMC)
30933383	Sk-68 39	ACYG	12.039				22580		B2.5Ia (LMC)
31105740	TYC 9161-925-1	ACYG	12.010				24970		B0.5Iae (LMC)
31181554	HD 269050	ACYG	11.540				25000		B0Ia(e?) (LMC)
31674330	GJ 127.1	-	11.394			0	16860	-2.75	DA3.0
31867144	HD 22252	SPB	5.806			223	12157	2.72	B8IV
33945685	HD 223118	ROT	8.250	2.835	273		10500	1.60	B9V
38602305	HD 27657	ROT	5.870	0.336	42		12448	2.13	B9III/IV; A2-A7m
40343782	HD 269101	ACYG?	12.030				21370		B3Iab; (LMC)
41331819	HD 43107	ROT	5.044	0.714	106	98	10886	2.04	B9.5III, B8V
47296054	HD 214748	SPB/ROT	4.180	0.836	202	180	13520	2.84	B8IVe (Be)
49687057	HD 220787	-	8.290			26	17379	3.54	B3III
53992511	HD 209522	BE	5.952			280	22570	3.51	B4IVe (Be)
55295028	HD 33599	BE	8.970			200	22570	4.44	B3p shell: (Be)
66497441	HD 222847	ELL	5.235			307	12000	2.24	B8.5Vnn
69925250	V* HN Aqr	BCEP+SPB	11.470			45	22909	4.31	B0/1
89545031	HD 223640	SXARI	5.180	0.266	36	27	12462	2.20	B9SiSrCr*
92136299	HD 222661	ROT+FLARE?	4.483	2.251	225	120	11108	1.73	B9.5IV
115177591	HD 201108	ROT	6.900	1.736	345		10158	2.17	B8IV/V
118327563	CD-38 222	ROT(+FLARE?)	10.260	4.372	54		26300	1.42	sdB
139468902	HD 213155	ROT	6.924	2.199	264		9628	1.64	B9.5V
141281495	HD 37854	ROT	8.100	0.334	48		10500	1.96	B9/9.5V
147283842	HD 205805	-	10.180				25000	1.67	sdB4
149039372	HD 34543	SPB?	8.370				11583	2.12	B8V
149971754	HD 41297	SPB	10.000				13520	2.57	B8IV
150357404	HD 45796	SPB/ROT?	6.248	0.640	114		13775	2.61	B6V
150442264	HD 46792	EB	6.140				16605	3.42	B3(V)k
152283270	HD 208433	ROT?/EA	7.440	0.434	69		10500	2.04	B9.5V
167045028	HD 45527	EB?	9.910	0.329	62		11000	2.27	B9IV
167415960	HD 48467	-	8.270				10613	2.19	B8/9V
167523976	HD 49193	SPB	8.940				23000	3.97	B2V
169285097	CD-35 15910	sdB Hybrid	11.000				28390	1.50	sdB He1
176935619	HD 49306	ROT	6.700	2.748	326		10082	1.71	B9.5/A0V
176955379	HD 49531	ROT	8.910	2.994	414		11900	2.13	B8/9Vn
177075997	HD 51557	ROT?	5.393	0.352	89	124	12325	2.72	B7III
179308923	HD 269382	ACYG+EB?	10.815				44500		O9.5Ib (LMC)
179574710	HD 271213	ACYG	12.310				23790		B1Iak (LMC)
179637387	[OM95]LH47-373A	ACYG?	11.970				20300		B1Ib (LMC)
179639066	HD 269440	ACYG	11.378				22240		B1.5Ia (LMC)
181043970	HD 5148	EA	10.640				11000	1.41	B9/A2IV:
182909257	HD 6783	SXARI	7.940	0.319	36	30	12941	2.11	B8Si
197641601	HD 207971	ROT?	3.010	0.201	68	55	11984	2.92	B8IV-Vs
206362352	HD 223145	SPB	5.161			240	17163	3.03	B2.5V
206547467	HD 210780	ROT	8.340	0.233	16		12500	1.61	B9.5/A0V
207176480	HD 19818	BE	9.060				11710	1.59	B9/A0Vne: (Be)
207235278	HD 20784	ELL	8.280	0.558	187		9175	2.45	B9.5V
220430912	HD 31407	EA	7.690				19648	3.76	B2/3V
224244458	HD 221507	SXARI/FLARE	4.370	0.522	57	21	12380	2.00	B9.5IVpHg:Mn:Eu:
229013861	HD 208674	ROT?	7.920	0.423	35		14555	2.04	B9.5V
230981971	HD 10144	BE	0.460			225	20760		B4V(e) (Be)
231122278	HD 29994	SPB	8.110				11900	2.08	B8/9V
238194921	HD 24579	ROT/SPB	8.060	0.727	134		13200	2.56	B7III

TIC	Name	Var. Type	V mag	$\nu_{\rm rot}$ (d^{-1})	v_e (km/s)	$v\sin i$ (km/s)	$T_{\rm eff}$ (K)	$\log\frac{L}{L_\odot}$	Sp. Type
259862349	HD 16978	ROT?	4.106	0.402	53	90	10003	1.79	B9V
260128701	HD 42918	SPB	7.950				16289	3.00	B4V
260131665	HD 42933	EB	4.810			170	25981	4.58	B0.5:III?np + B0.5/3:
260368525	HD 44937	ROT?	8.190	1.194	241		10500	2.24	B9.5V
260540898	HD 46212	ROT?	8.260	0.562	117		12400	2.56	B8IV
260640910	HD 46860	BE	5.707			200	13520	2.70	B8III (Be)
260820871	HD 218801	EP	8.990				10500	1.92	B9.5Vn:
261205462	HD 40953	SPB	5.451			23	11243	1.93	B9V
262815962	HD 218976	ROT	8.120	0.369	40		9846	1.60	B9.5/A0V
270070443	HD 198174	SXARI	5.854	0.395	64	72	13217	2.46	B7IIIp
270219259	HD 209014	BE/MAIA	5.620			350	13520	2.96	B8III shell (Be)
270557257	HD 49835	ROT?	8.560	2.475	253		10500	1.65	B9.5V
270622440	HD 224112	-	6.828			35	12268	2.32	Blend with 270622446
270622446	HD 224113	EA	6.087			135	13665	2.70	B7(V) + B9(V)
271503441	HD 2884	ROT	4.335	3.056	282	140	11576	1.73	B8/A0
271971626	HD 62153	ROT/MAIA	7.020	0.215	38		11783	2.33	B9IV
276864600	HD 269777	ACYG	11.060				21370		B3Ia (LMC)
277022505	HD 269786	ACYG	11.180				28000		B1I (LMC)
277022967	HD 37836	ACYG	10.660				28000		B0e(q)I (LMC)
277099925	HD 269845	ACYG	11.790				22580		B2.5Ia (LMC)
277103567	HD 37935	ROT/ELL	6.281	1.496	361		9940	2.30	B9.5V (Be)
277172980	HD 37974	ACYG	10.959				28000		B0.5e (LMC)
277173650	HD 269859	ACYG	10.730				23790		B1.5Ia (LMC)
277298891	Sk-69 237	ACYG	12.080				24625		B1Ia (LMC)
277982164	HD 54239	ROT	5.459	1.266	248		9938	2.12	B9.5/A0III/IV
278683664	HD 47770	ROT?	8.490	1.701	268		9012	1.76	B9.5V
278865766	HD 48971	-	8.280				9743	1.93	B9V
278867172	HD 49111	-	8.490				14273	2.11	B9.5V
279430029	HD 53048	ROT	7.920	1.784	554		18950	3.64	B5/7Vn(e:) (Be)
279511712	HD 53921	ELL	5.600	0.605	141		13800	2.84	B9III+B8V
279957111	HD 269582	-	12.597				30200		Ofpe/WN9 (LMC)
280051467	HD 19400	SXARI	5.497	0.229	36	64	14117	2.56	B8III/IV Hewk
280684074	HD 215573	SPB	5.313	0.563	104	13	13960	2.66	B6V
281703963	HD 4150	MAIA	4.365			105	9822	2.06	A0IV/B9Vp((SiFe))
281741629	CD-56 152	BE	10.180			180	19000	4.59	sdB?/Be?
293268667	HD 47478	SPB	8.500	3.390	455		10765	1.93	B9V
293271581	Hen 3-15	EB	12.502				11710	0.67	Bem RR Pic (Nova)
293973218	HD 54967	SPB	6.470			34	22570	3.47	B3III
294747615	HD 30612	SXARI	5.515	0.192	30	30	13661	2.50	B8II/IIIp:Si:
294872353	HD 270754	ACYG	11.260				19910		B1.5Ia: (LMC)
300010961	HD 55478	ROT/MAIA	8.060	0.683	122		11144	2.24	B8III
300325379	HD 58916	ROT	8.010	1.838	268		11710	2.15	B9Vn
300329728	HD 59426	ELL/ROT	8.420	0.411	51		11710	2.02	B9V
300744369	HD 63928	ROT	8.700	0.957	102		11710	1.88	B9V
300865934	HD 64484	-	5.774				10707	2.14	B9V
306672432	HD 67252	ROT?	8.530	1.090	119		13520	2.15	B8/9V
306824672	HD 68221	SPB?	8.650				11710	2.32	B9V
306829961	HD 68520	SPB	4.400			10	14090	3.44	B5III
307291308	HD 71066	SXARI	5.617	0.387	62	2	11821	2.25	B9pMnHg
307291318	HD 71046	-	5.329			69	12102	2.37	B9III/IV
307993483	HD 73990	SPB?	6.870	3.697			10221	2.02	B7/8V
308395911	HD 66591	SPB	4.797			43	16983	2.96	B3IV
308454245	HD 67420	MAIA	8.250				11710	2.15	B9V
308456810	HD 67170	ROT	8.110	0.251	38		13520	2.43	B8III/IV
308537791	HD 67277	ROT+MAIA	8.260	0.527	78		13520	2.41	B8III
308748912	HD 68423	-	6.313				15330	2.86	B7IVek (Be)
309702035	HD 271163	ACYG	9.984				21370		B3Ia (LMC)
313934087	HD 224990	SPB	5.023			15	16100	3.08	B4III
327856894	HD 225253	LPB?	5.581				13123	2.64	B8IV/V
349829477	HD 61267	-	8.330				10000	1.72	B9/A0IV
349907707	HD 61644	EA	8.410				15000	2.76	B5/6IV
350146577	HD 63204	SXARI	8.310	0.544	78		10505	1.95	B9Si
350823719	HD 41037	EB	9.460			215	18700	3.60	B3V
354671857	HD 14228	ROT?	3.570	2.908	375	200	12687	2.18	B8IV-V
355141264	HD 208495	-	8.860				9945	1.58	B9.5V

TIC	Name	Var. Type	V mag	$\nu_{\rm rot}$ ($\rm d^{-1}$)	v_e (km/s)	$v \sin i$ (km/s)	$T_{\rm eff}$ (K)	$\log \frac{L}{L_\odot}$	Sp. Type
355477670	HD 220802	ROT?	6.210	0.272	37		11206	2.03	B9V
355653322	HD 224686	ROT	4.470	1.266	274	275	11710	2.49	B9IIIn (Be)
358232450	HD 6882	EA	3.967			111	13471	2.41	B6V + B9V
358466708	CD-60 1931	ROT	8.090	1.661	280	223	12814	2.43	B8III
358467049	CPD-60 944	SXARI	8.756	0.265	30		12600	2.07	B8pSi
358467087	CD-60 1929	SPB?	8.520			43	12543	2.26	B8.5IV
364323837	HD 40031	SPB?	9.270			65	14000	3.08	sdB, B6III
364398190	CD-60 1978	ROT	8.750	0.760	101	68	12337	2.16	B8.5IV-V
364398342	HD 66194	BE	5.810			200	20632	3.76	B2IVn(e)p(Si) (Be)
364421326	HD 66109	ROT?	8.190	1.976	385		11710	2.40	B9.5V
369397090	CD-30 19716	-	12.860				39811	1.43	sdB
369457005	HD 197630	SPB?	5.474				11511	1.99	B8/9V
370038084	HD 26109	-	8.580				11710	1.62	B9.5/A0V
372913233	HD 65950	-	6.870			26	12842	2.88	B8.5IIIpMnHg
372913582	CD-60 1954	SPB?	8.590			188	10579	2.13	B9.5V
372913684	HD 65987	SXARI	7.590	0.685	163	13	12600	2.70	B9.5IVpSi
373843852	HD 269525	ACYG	12.780				28000		B0: (LMC)
389921913	HD 270196	ACYG	11.600				22875		B1.5Ia (LMC)
391810734	HD 269655	ACYG	12.200				28800		B0Ia (LMC)
391887875	HD 269660	ACYG	11.190				21430		B1.5Ia (LMC)
404768847	VFTS 533	ACYG?	11.820			57	19275		B1.5Ia+qp (LMC)
404768956	NGC2070 Mel 12	ACYG?	11.996				28510		B0/0.5Ia (LMC)
404796860	HD 269920	ACYG	11.650				18950		B5Ia (LMC)
404852071	Sk-69 265	ACYG	11.880				21370		B3Ia (LMC)
404933493	HD 269997	ACYG	11.200				22580		B2.5Ia (LMC)
404967301	HD 269992	ACYG	11.220				18020		B2.5:Ia: (LMC)
410447919	HD 64811	ROT?	8.450	0.219	159		17100	4.20	B4III
410451677	HD 66409	SXARI	8.410	0.488	67	34	12987	2.28	B8.5IV(HgMn)?
419065817	HD 1256	ROT/ELL?	6.488	1.474	186	166	14280	2.37	B6III/IV
425057879	HD 269676	EB/ELL?	11.550			120	41000		O6+O9 (LMC)
425064757	HD 269696	EA	11.138				42000		sdO (LMC)
425081475	HD 269700	ACYG	10.540				23790		B1.5Iaeq (LMC)
425083410	HD 269698	ACYG	12.220				40400		O4If (LMC)
425084841	TYC 8891-3638-1	ACYG	12.180			62	23660		B1Ia (LMC)
441182258	HD 210934	SPB/ROT?	5.430	1.274	235	56	12526	2.47	B8III
441196602	HD 211993	ROT?	8.200	0.144	20		10750	1.96	B8/9V
469906369	HD 212581	MAIA	4.495			200	11271	2.18	B9.5IVn

types are caused by the opacity mechanism in the ionization zone of iron-group elements (Dziembowski et al. 1993). The β Cep stars are hotter (20000–32000 K) and pulsate with frequencies in the range 4–12 $\rm d^{-1}$, while the SPB stars are cooler (11000-19000 K) and pulsate with frequencies in the range 0.3–3 $\rm d^{-1}$.

In the GCVS, SPB stars are given the variability type LPB ("long-period B-star"). The reason for the different designation is that the GCVS wisely tries to avoid naming a variable type according to a specific interpretation of the cause of the light variation. If a much better interpretation for SPB light variations where to be found, for example, then the class will have to be renamed. However, since the designation LPB has fallen into disuse, SPB is used instead.

The ACYG variables are nonradially pulsating B-type supergiants. The multiple periods range from several days to several weeks. The B supergiants observed by *TESS* are all members of the Large Magellanic Cloud (LMC). With few exceptions, the light curves of all the LMC supergiants matched those expected for the ACYG variables.

The Be variables are B stars which show, or have shown, emission in Hα or other Balmer lines. This can include many different types of object, including supergiants, in which the emission is thought to be due to different physical mechanisms. The "classical Be stars" are a narrower set confined to stars in the main sequence band. Some Be stars show large, frequent outbursts in the light curve attributed to the sudden ejection of circumstellar material (GCAS variables). Others are less active and show quasi-periodic variations with timescales in the range 0.5–2 d, usually attributed to multiple nonradial pulsations and/or obscuration by circumstellar material. In the GCVS, the designation BE is used to describe these stars. The photometric variability type BE should not be confused with the spectroscopic classification "Be" which designates emission in some Balmer lines.

The EA and EB variables are eclipsing binaries. In EA variables it is possible to specify the beginning and end of eclipses. Between eclipses the light is more-or-less constant. On the other hand, the EB eclipsing variables are close binaries where the variation is practically sinusoidal with no constant light. The EP stars show very small eclipses which may be attributed to a planet or sub-stellar companion.

The MAIA type is a new class which was introduced by Balona et al. (2015, 2016). These are B stars which show many high-frequency peaks similar to those seen in BCEP or δ Scuti variables (called DSCT in the GCVS). However, they are too cool to be classified as BCEP and too hot to be DSCT. Whether or not they deserve a separate class remains to be seen. These stars may be related to the "FaRPB" stars (Mowlavi et al. 2016) which also show high frequencies and lie between the β Cep and δ Scuti variables. The FaRPB stars, however, are all rapidly-rotating stars. The evidence suggests that MAIA stars are not rapid rotating stars (Balona et al. 2016).

Some subdwarf B stars (sdB stars) are also known to be multiperiodic variables. There are two classes: the V361 Hya and the V1093 Her stars. V361 Hya stars are short-period pulsating sdB stars with $24000 < T_{\rm eff} < 40000$ K and $\log g < 5.8$ (less compact than white dwarfs). They have multiple periods in the range 60–400 s (200–1500 $\rm d^{-1}$). They are also known as EC 14026 stars. The V1093 Her stars are in the same general area of the H-R diagram, but somewhat cooler and less compact. They are long-period (1800–9000 s or 10–50 $\rm d^{-1}$) analogues of the V361 Hya stars and are also known as PG 1716 stars.

Table 1 lists our assigned variability type in the third column. Where the star seems constant or no definite assignment is possible, a dash is used.

5 EFFECTIVE TEMPERATURE

The effective temperature, $T_{\rm eff}$, may be estimated in several different ways, sometimes giving very different results. Literature values of $T_{\rm eff}$ were chosen according to the following order of descending priority.

Whenever possible, estimates of $T_{\rm eff}$ from modelling the spectrum star were chosen (Urbaneja et al. 2017; Gullikson et al. 2016). Failing this, an estimate based on narrow-band photometry (i.e.Strömgren $uvby\beta$ or Geneva photometry) was used (Pauznen et al. 2005; Silaj & Landstreet 2014). For some stars, Strömgren photometry was available, but no value of $T_{\rm eff}$ had yet been derived. In such cases we estimated $T_{\rm eff}$ by de-reddening the star using the method described by Crawford (1978) and then applying the calibrations of Balona (1994) to obtain $T_{\rm eff}$.

Next in priority were methods using the spectral energy distribution (SED) from wide-band photometry, usually UBVRI (Chandler et al. 2016). There can be problems with this method if measurements in the U band are missing, so $T_{\rm eff}$ from SED was selected only if it agreed reasonably well with the temperature from the spectral type. If not, or if no $T_{\rm eff}$ measurements could be found, the spectral type itself was used to estimate $T_{\rm eff}$ from the table of Pecaut & Mamajek (2013). For emission-line stars the $T_{\rm eff}$ from the spectral type was used instead of photometric methods.

The error in $T_{\rm eff}$ clearly depends on the method used, but we can obtain an approximate overall value for B stars from the PASTEL catalogue (Soubiran et al. 2016). The errors increase with $T_{\rm eff}$ ranging from 500 to 1500 K. We adopt a standard error of 1000 K as reasonable overall estimate.

6 LUMINOSITIES AND RADII

From the *Gaia* DR2 parallax π (Gaia Collaboration et al. 2016), the absolute magnitude is calculated using $M_V = V_0 + 5(\log_{10}\pi + 1)$, where V_0 is the reddening-free V magnitude. The reddening correction was derived from a three-dimensional reddening map with a radius of 1200 pc around the Sun and within 600 pc of the galactic midplane as calculated by Gontcharov (2017). For more distant stars, a simple reddening model is used (see Eq. 20 of Brown et al. 2011), but adjusted so that it agrees with the 3D map at 1200 pc.

The absolute bolometric magnitude is given by $M_{\rm bol} = M_V + {\rm BC}_V - M_{\rm bol\odot}$, where $\rm BC_V$ is the bolometric correction in V and $M_{\rm bol\odot} = 4.74$ is the absolute bolometric magnitude of the Sun. Finally, the luminosity relative to the Sun is found using $\log L/L_\odot = -0.4M_{\rm bol}$. From the error in the *Gaia* DR2 parallax, the typical standard deviation in $\log(L/L_\odot)$ is estimated to be about 0.05 dex, allowing for standard deviations of 0.01 mag in the apparent magnitude, 0.10 mag in visual extinction and 0.02 mag in the bolometric correction in addition to the parallax error.

From the luminosity and effective temperature, the stellar radius, $R/R_\odot$, can be found. For stars where the rotational modulation frequency $\nu_{\rm rot}$ is available, the equatorial rotational velocity v_e can be determined. Table 1 shows $\log L/L_\odot$. For those stars with known $\nu_{\rm rot}$, v_e is also shown.

In addition to the *TESS* stars, we have examined the light curves of *Kepler* and *K2* data for possible rotational modulation. Table 2 lists the measurements and stellar parameters obtained in the same way. Fig. 1 shows the main sequence stars in Tables 1 and 2 in the theoretical H-R diagram.

7 ROTATIONAL MODULATION

The frequencies listed as $\nu_{\rm rot}$ in Tables 1 and 2 are all highly significant according to the false alarm probability (Scargle 1982). Probabilities that the specified frequency is due to noise are always less than 10^{-6} and the ratio of the peak amplitude to background noise level is always greater than 10. The typical peak amplitude is around 135 ppm.

As already mentioned, one test for rotational modulation is to compare the equatorial rotational velocity, v_e, obtained from $\nu_{\rm rot}$ and the stellar radius, with $v \sin i$. For this purpose, values of $v \sin i$ in Tables 1 and 2 were obtained from the catalogue of Glebocki & Gnacinski (2005). Fig. 2 shows $v \sin i$ as a function of v_e for the *TESS* main sequence stars identified as ROT (solid circles) or SXARI (open circles) in Tables 1 and 2. As expected, most stars fall below the $\sin i = 1$ line. If the variation is not related to rotation, one would have expected both sides of the $\sin i = 1$ line to be populated.

The typical error in $v \sin i$ for B stars can be estimated from the catalogue of Glebocki & Gnacinski (2005). The error increases with $v \sin i$ and ranges between 0 and 60 $\rm km\,s^{-1}$. A representative value of $\sigma_{v \sin i} = 30\,\rm km\,s^{-1}$ is reasonable. From the error in $\log L/L_\odot$ and $T_{\rm eff}$ it is easy to calculate the error in v_e. This error depends almost entirely on the error in $T_{\rm eff}$. The contribution from the luminosity error is small while the contribution from the error in $\nu_{\rm rot}$

Table 2. Additional rotational variables identified from the light curves of the *Kepler* and *K2* missions.

KIC/EPIC	Name	Var. Type	V mag	$\nu_{\rm rot}$ (d^{-1})	v_e (km/s)	$v\sin i$ (km/s)	$T_{\rm eff}$ (K)	$\log\frac{L}{L_\odot}$	Sp. Type
EPIC 210788932	HD 23016	ROT	5.690	1.802	351	260	11463	2.36	B8Ve?
EPIC 211116936	HD 23324	SPB/ROT	5.640	1.543	251	206	12218	2.32	B8:IV/V
EPIC 211028385	HD 23753	ROT	5.450	1.808	309	292	11899	2.31	B8IV/V
EPIC 211054599	HD 23964	SXARI	6.740	0.633	77	20	10190	1.75	B9.5VspSiSrCr
EPIC 210964459	HD 26571	SXARI	6.120	0.063	22	22	11430	2.85	B9IIIp:(Si)
EPIC 202061205	HD 253049	ROT	9.620	0.294	90	184	22570	3.93	B3III
EPIC 211311439	HD 74521	SXARI	5.660	0.144	29	18	10615	2.26	B9pSiCr
EPIC 201232619	HD 97991	ROT	7.410	0.496	323	137	9956	3.16	B2/3V
EPIC 204760247	HD 142883	ROT	5.841	1.103	254	19	9648	2.21	B3V
EPIC 204134887	HD 142884	SXARI	6.777	1.245	200	138	9979	1.95	kB8hB4HeB9V Si4200
EPIC 204348206	HD 143600	ROT	7.330	3.922	452	265	9087	1.50	B9Vann
EPIC 204095429	HD 144844	SXARI	5.880	0.116	25	98	9362	2.11	B9MnPGa
EPIC 202909059	HD 145482	ROT	4.567	0.172	59	178	11131	2.81	B2.5III
EPIC 204964091	HD 147010	SXARI	7.400	0.255	25	25	9092	1.38	B9SiCrSr*
EPIC 205417334	HD 148860	ROT	8.040	0.920	177	257	9566	2.03	B9.5V
KIC 8351193	HD 177152	ROT	7.570	1.757	168	180	10500	1.59	A0VkB8mB7 λ Boo
EPIC 217692814	HD 177015	ROT	7.800	1.139	447	202	10567	2.83	B5V(e)
KIC 8087269	ILF1 +43 30	ROT	11.710	1.610	268	271	14500	2.63	B5
KIC 9278405	ILF1 +45 284	ROT	10.160	1.805	194	110	11100	1.79	B9
KIC 4056136	BD+38 3580	ROT	9.550	2.370	351	227	10500	1.97	B9IV-Vnn
KIC 9468611		ROT	13.144	2.193	290	263	11200	1.98	B9IV
KIC 6128830	BD+41 3394	SXARI	9.190	0.206	56	15	12600	2.82	B6pHgMn
KIC 7974841	HD 187139	ROT	8.160	0.255	22	33	10650	1.55	B8V
KIC 5477601		ROT	12.793	0.192	25	88	11950	2.12	B9V
KIC 5130305	HD 226700	ROT	10.210	2.151	330	155	10670	2.03	B9
KIC 8324268	HD 189160	SXARI	7.900	0.498	72	31	11370	2.09	B9pSiCr
KIC 8389948	HD 189159	ROT	9.140	0.994	158	142	10240	1.99	B9.5IV-V
KIC 5479821	HD 226795	ROT	9.890	0.588	119	85	14810	2.84	B8
EPIC 206326769	HD 211838	SXARI	5.346	0.893	389	66	10634	2.93	B8IIIp:(MnHg?)
EPIC 206097719	HD 213781	SXARI	9.000	0.181	103	34	9135	2.89	B7Si

is entirely negligible. The typical value for the error in the derived equatorial rotational velocity is $\sigma_{v_e} \approx 40\,\mathrm{km\,s^{-1}}$. These error bars are shown in Fig. 2.

Fig. 2 allows the angle of inclination, i, to be estimated for a particular star since $\sin i = v\sin i/v_e$. The variance in $\sin i$ is given by

$$\mathrm{var}(\sin i)/\sin^2 i = \mathrm{var}(v\sin i)/(v\sin i)^2 + \mathrm{var}(v_e)/v_e^2.$$

which means that the error in $\sin i$ increases rapidly with decreasing rotation rate. Thus one expects that as v_e tends to zero, more and more stars will be pushed above the $\sin i = 1$ line due to the increasing errors, as seen in Fig. 2. Only rapidly rotating stars are useful in estimating $\sin i$.

8 FLARE STARS

Optical stellar flares are usually associated with active M dwarfs which can dramatically increase in brightness over a broad wavelength range from X-rays to radio waves for anywhere from a few minutes to a few hours. The rapid rise in brightness is followed by a slow decay with a timescale from minutes to hours. The largest change in brightness occurs at short wavelengths: a rise of one magnitude in the V band is typically accompanied by a rise of five magnitudes in the U band. The amplitudes are much lower in the very wide band used in the *TESS* and *Kepler* observations.

Flares in the Sun are caused by energy released by the re-connection of magnetic field lines in the outer atmosphere. The energies released in solar flares are in the range 10^{29}–10^{32} ergs. Flares in active M dwarfs are typically 10–1000 times more energetic than solar flares. Although we have a very limited understanding of stellar flares, it is thought that the underlying mechanism is essentially the same as in the Sun.

The *Kepler* mission has resulted in the discovery of "superflares" in solar-type stars with energies in the range 10^{33}–10^{36} ergs (Maehara et al. 2012). More surprisingly, flaring was found in about 2.5 percent of A stars (Balona 2012, 2013, 2015). Spectroscopic observations of the A-type flare stars suggest significant contamination by field stars in the *Kepler* aperture and that many of the stars are spectroscopic binaries (Pedersen et al. 2017). The possibility that the flares originate in a companion certainly cannot be discounted. However, it should be noted that the flares associated with A stars are 100–1000 times more energetic than those in typical M or K dwarfs (Balona 2015), suggesting that they may originate in the A star and not on a late-type companion.

In the course of inspection of the *TESS* light curves, we came across three stars which appear to flare (Fig. 3). TIC 92136299 is a normal B9.5IV star with clear periodic variations suggestive of rotational modulation. The periodogram shows a main peak at $2.251\,\mathrm{d}^{-1}$ and its first harmonic. In addition, there is a third peak at $2.642\,\mathrm{d}^{-1}$ which

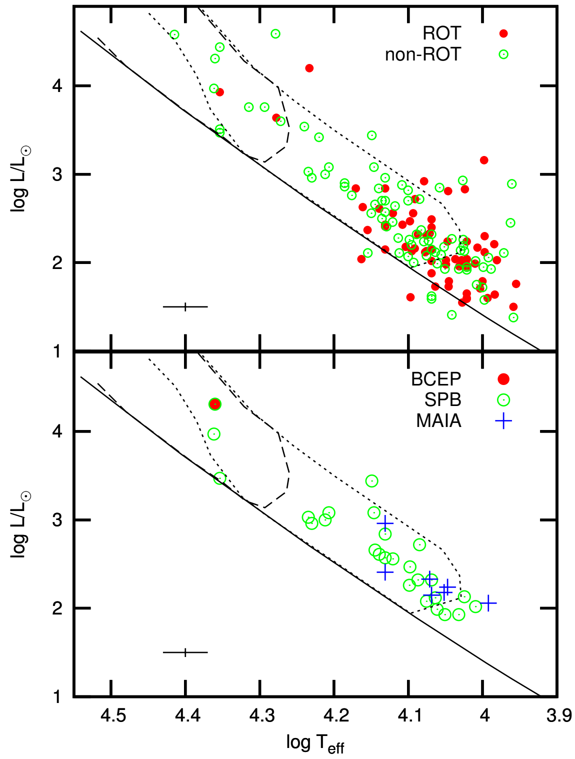

Figure 1. The theoretical H-R diagram for *TESS*, *Kepler* and *K2* main sequence stars. The top panel shows stars identified as possible rotational variables (filled circles). The open circles are other main sequence stars (including the SXARI rotational variables). In the bottom panel pulsating variable stars in the *TESS* field are shown. The filled circle is the only BCEP star in the sample, HN Aqr. The open circles are stars classified as SPB variables. The crosses are MAIA stars. The solid line is the zero-age main sequence from solar-abundance models by Bertelli et al. (2008). The dashed and dotted areas are the theoretical BCEP and SPB instability regions from Miglio et al. (2007). The cross at the bottom shows the typical 1-σ error bars.

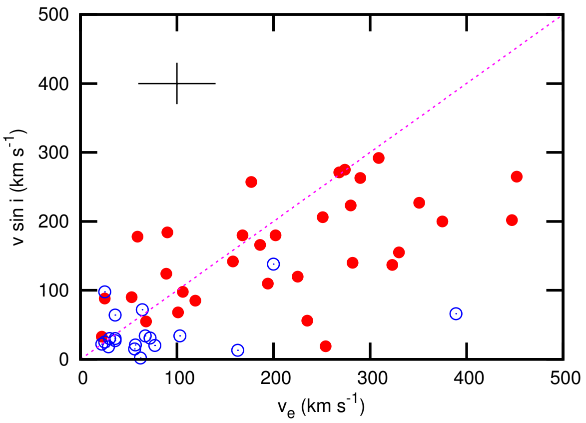

Figure 2. The projected rotational velocity, $v \sin i$, as a function of equatorial rotational velocity, v_e, for stars in the *TESS*, *Kepler* and *K2* fields (filled circles). The open circles are SXARI stars which are rotational variables due to chemical abundance variations across the surface. The straight line has unit slope, corresponding to $\sin i = 1$. The cross at the top left is the approximate 1-σ error bars.

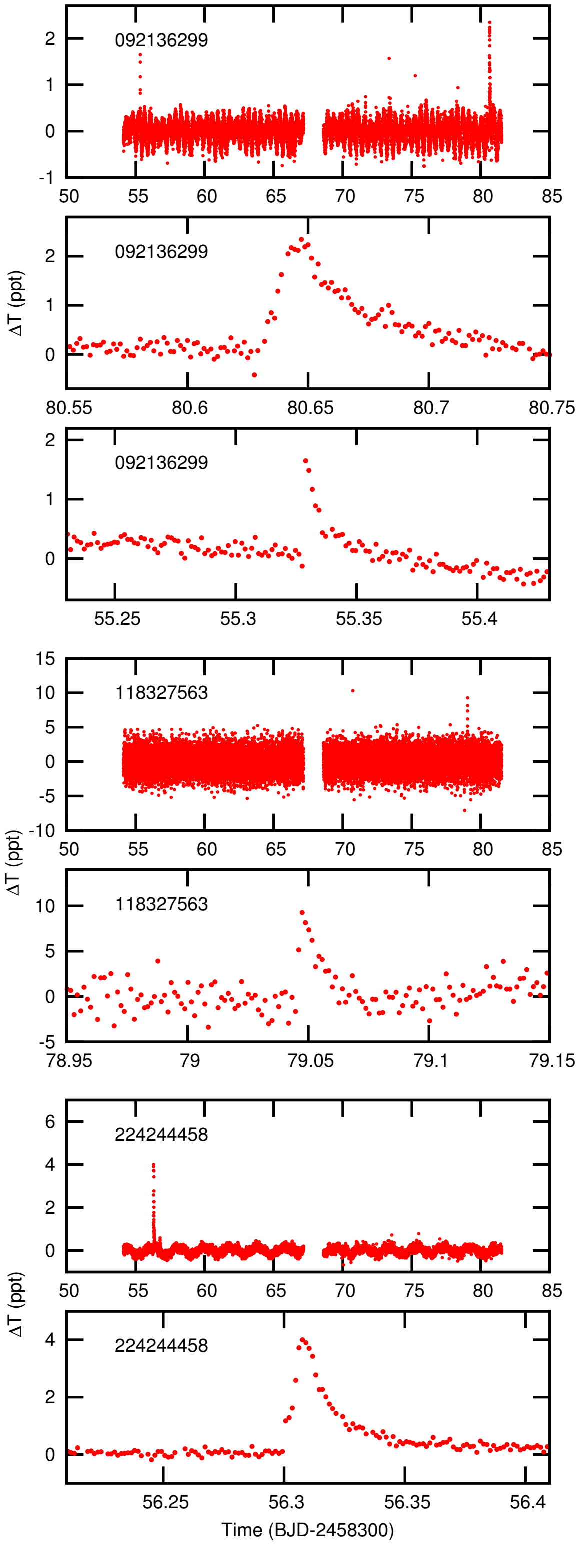

Figure 3. Light curves of three stars (TIC numbers given) which appear to show one or more flares. The units for the light variation are parts per thousand (ppt).

could be interpreted as a second “spot” in a differentially-rotating star. Two flare-like events can be seen which have the typical sharp rise and slow decay of a stellar flare. According to Chini et al. (2012), the star is not a spectroscopic binary.

TIC 92136299 (ω^2 Aqr A) has a close companion, (ω^2 Aqr B) with spectral type A5IVpec with the H&K CaII lines in emission (Gahm et al. 1983). The stars are separated by 5 arcsec and magnitude difference of 6 mag. The pair is an X-ray source (Makarov 2003).

A flare is also found in TIC 118327563 which is a subdwarf B star. Bagnulo et al. (2015) was unable to detect a significant magnetic field. The rapid light variation of 4.372 d^{-1} is clearly seen in the light curve. The periodogram shows two closely-spaced peaks at 4.372 and 4.203 d^{-1} and their first harmonics.

The flare on TIC 224244458 (β Scl) is very interesting as this is a HgMn star. The HgMn stars are chemically peculiar stars containing an excess of P, Mn, Ga, Sr, Yt, Zr, Pt and Hg. They lack a strong dipole magnetic field and are slow rotators. For β Scl, Bychkov et al. (2009) quotes a (null) magnetic field measurement of 61 ± 36 G. Chini et al. (2012) found that the star is not a spectroscopic binary.

We can calculate the approximate flare energy from the area occupied by the flare in the light curve and the stellar luminosity. These turn out to be approximately 10^{36} ergs for TIC 92136299 and TIC 224244458 and 10^{35} ergs for TIC 118327563, which are all considerably larger than the most energetic flares in typical K or M dwarfs, but similar to the flare energies in A stars. This does not prove that the flares originate on B stars, but is an indication that this might be the case.

9 OTHER STARS OF INTEREST

The only β Cep star in the sample is TIC 69925250 (HN Aqr). *TESS* observations of the star are discussed by Handler et al. (2019).

There are 25 stars classified as SPB variables in the *TESS* data. The classification is based on the presence of multiple low-frequency peaks. In some stars one may interpret a strong peak and its harmonic as possibly due to rotation. These have been designated SPB/ROT variables and are treated as both SPB and rotational variables.

The 12 stars considered to be classical Be stars are designated in the last column of Table 1 by “(Be)”. Many of them display broad multiple peaks considered to be a result of nonradial pulsation or variable circumstellar obscuration. These are classified as BE variables, in accordance with the GVCS definition. In addition to the broad peaks, TIC 270219259 also shows a strong, sharp peak at 7.445 d^{-1}. The star is too cool for a BCEP, so we have classified it as BE/MAIA. Some stars (TIC 279430029, TIC 355653322) have only a single sharp peak and its harmonic which we therefore classify as ROT. TIC 47296054 has some harmonics of the fundamental frequency at 0.836 d^{-1}. There is a low-amplitude peak close to the subharmonic frequency, which might imply that it is also an SPB variable. TIC 308748912 does not have any significant peaks with frequencies higher than 0.5 d^{-1} and with amplitudes above 10 ppm.

Of the 7 stars classified as MAIA variables, three have $v \sin i$ measurements. This brings to 16 the number of suspected MAIA stars with known $v \sin i$, for which the mean is $< v \sin i >= 111 \pm 23\,\mathrm{km\,s}^{-1}$. This does not suggest that rapid rotation is an important factor, unlike the FaRPB stars.

TIC 169285097 is a known subdwarf pulsating B star (Holdsworth et al. 2014). The *TESS* data show that it pulsates in both long- and short periods (hybrid V361 Hya/V1093 Her star). There are dozens of peaks in the range $8 < \nu < 60\,\mathrm{d}^{-1}$, but also a few peaks in the range $220 < \nu < 250\,\mathrm{d}^{-1}$. The other sdB stars and the white dwarf TIC 31674330 appear to be constant.

Another class of interest are rotational variables with detected magnetic fields in the first *TESS* data release. These are being investigated by David-Uraz et al. (2019, in preparation).

10 CONCLUSIONS

For the last half-century the view that stars with radiative envelopes cannot sustain a magnetic field and are therefore devoid of starspots has been generally assumed. Suspicions that this was not the case have occasionally arisen, particularly from inspection of good ground-based photometric time series of δ Sct and β Cep stars, where the presence of significant low frequencies has sometimes been noted. However, owing to the fact that the rotational periods of A and B stars are close to one day, it is very difficult to detect low-amplitude rotational modulation of A and B stars in ground-based photometry from a single site.

With the advent of precise time-series photometry from space it has become apparent that rotational modulation is very likely present in about half the A stars in the *Kepler* field (Balona 2013, 2017). This is demonstrated by the fact that the photometric period distribution closely matches the expected distribution from spectroscopic $v \sin i$ measurements (Balona 2013). Furthermore, the expected relation between the equatorial rotational velocity, v_e, estimated from the photometric period and $v \sin i$ is also present (Balona 2017).

There are very few B stars in the *Kepler* and *K2* fields (most of them are late B stars), too few to calculate the v_e distribution and compare it with the v_e distribution expected from spectroscopic $v \sin i$ measurements from field stars in the same temperature range. Balona (2016) was able to identify presumed rotational modulation in many B stars observed with the *K2* mission, but for the most part $v \sin i$ measurements were not available to test the relationship with v_e.

In this paper we examined the light curves of 160 B stars observed by *TESS* and classified them according to variability type. It appears that a large fraction of these stars may be rotational variables without any known chemical peculiarity. Balona (2016) had already arrived at the same conclusion from a sample of *K2* B stars.

Using *Gaia* parallaxes, the luminosities of these main sequence stars were estimated, from which the radii can be found. From the radii and the photometric periods, the equatorial rotational velocities can be determined. The expected relationship between projected rotational velocity and the equatorial rotational velocity is found, confirming that the photometric periods are consistent with rotation.

Out of the 112 main-sequence B stars observed by *TESS*, 45 were classified as rotational variables. This fraction (about 40 percent) is similar to the fraction of rotational variables found among the A stars (Balona 2013) and a confirmation of a similar result from B stars in the *K2* field (Balona 2016). Rotational variability appears to be the most common type of light variation among A and B main sequence stars. None of these variables are known to be chemically peculiar.

This result calls into question current models of the outer layer of stars with radiative envelopes. Cantiello et al. (2009) and Cantiello & Braithwaite (2011) have suggested that magnetic fields produced in subsurface convection zones could appear on the surface. Thus localized magnetic fields could be widespread in those early type stars with subsurface convection. Magnetic spots of size comparable to the local pressure scale height are predicted to manifest themselves as hot, bright spots (Cantiello & Braithwaite 2011). Recent observations from space indicate that bright spots may have been detected in some O stars (Ramiaramanantsoa et al. 2014; David-Uraz et al. 2017; Ramiaramanantsoa et al. 2018). It is also possible that differential rotation in the A and B stars may be sufficient to create a local magnetic field via dynamo action (Spruit 1999, 2002; Maeder & Meynet 2004). Whether or not any of these ideas relates to rotational modulation as observed in A and B stars requires further work.

ACKNOWLEDGMENTS

LAB wishes to thank the National Research Foundation of South Africa for financial support. GMM acknowledges funding by the STFC consolidated grant ST/R000603/1. GH and SC gratefully acknowledge funding through grant 2015/18/A/ST9/00578 of the Polish National Science Centre (NCN). GAW acknowledges Discovery Grant support from the Natural Sciences and Engineering Research Council (NSERC) of Canada. ADU acknowledges the support of the Natural Science and Engineering Research Council of Canada (NSERC).

This paper includes data collected by the *TESS* mission. Funding for the *TESS* mission is provided by the NASA Explorer Program. Funding for the *TESS* Asteroseismic Science Operations Centre is provided by the Danish National Research Foundation (Grant agreement no.: DNRF106), ESA PRODEX (PEA 4000119301) and Stellar Astrophysics Centre (SAC) at Aarhus University. We thank the *TESS* and TASC/TASOC teams for their support of the present work.

This research has made use of the SIMBAD database, operated at CDS, Strasbourg, France.

This work has made use of data from the European Space Agency (ESA) mission *Gaia* (`https://www.cosmos.esa.int/gaia`), processed by the *Gaia* Data Processing and Analysis Consortium (DPAC, `https://www.cosmos.esa.int/web/gaia/dpac/consortium`). Funding for the DPAC has been provided by national institutions, in particular the institutions participating in the *Gaia* Multilateral Agreement.

The data presented in this paper were obtained from the Mikulski Archive for Space Telescopes (MAST). STScI is operated by the Association of Universities for Research in Astronomy, Inc., under NASA contract NAS5-2655.

REFERENCES

Bagnulo S., Fossati L., Landstreet J. D., Izzo C., 2015, A&A, 583, A115
Balona L. A., 1994, MNRAS, 268, 119
—, 2012, MNRAS, 423, 3420
—, 2013, MNRAS, 431, 2240
—, 2015, MNRAS, 447, 2714
—, 2016, MNRAS, 457, 3724
—, 2017, MNRAS, 467, 1830
—, 2018, MNRAS, 479, 183
Balona L. A., Baran A. S., Daszyńska-Daszkiewicz J., De Cat P., 2015, MNRAS, 451, 1445
Balona L. A., Engelbrecht C. A., Joshi Y. C., Joshi S., Sharma K., Semenko E., Pandey G., Chakradhari N. K., Mkrtichian D., Hema B. P., Nemec J. M., 2016, MNRAS, 460, 1318
Bertelli G., Girardi L., Marigo P., Nasi E., 2008, A&A, 484, 815
Brown T. M., Latham D. W., Everett M. E., Esquerdo G. A., 2011, AJ, 142, 112
Bychkov V. D., Bychkova L. V., Madej J., 2009, MNRAS, 394, 1338
Cantiello M., Braithwaite J., 2011, A&A, 534, A140
Cantiello M., Langer N., Brott I., de Koter A., Shore S. N., Vink J. S., Voegler A., Lennon D. J., Yoon S., 2009, A&A, 499, 279
Chandler C. O., McDonald I., Kane S. R., 2016, AJ, 151, 59
Charbonneau P., 2014, ARA&A, 52, 251
Chini R., Hoffmeister V. H., Nasseri A., Stahl O., Zinnecker H., 2012, MNRAS, 424, 1925
Chowdhury S., Joshi S., Engelbrecht C. A., De Cat P., Joshi Y. C., Paul K. T., 2018, Ap&SS, 363, 260
Crawford D. L., 1978, AJ, 83, 48
David-Uraz A., Owocki S. P., Wade G. A., Sundqvist J. O., Kee N. D., 2017, MNRAS, 470, 3672
Dziembowski W. A., Moskalik P., Pamyatnykh A. A., 1993, MNRAS, 265, 588
Gahm G. F., Ahlin P., Lindroos K. P., 1983, A&AS, 51, 143
Gaia Collaboration, Prusti T., de Bruijne J. H. J., Brown A. G. A., Vallenari A., Babusiaux C., Bailer-Jones C. A. L., Bastian U., Biermann M., Evans D. W., et al., 2016, A&A, 595, A1
Glebocki R., Gnacinski P., 2005, VizieR Online Data Catalog, 3244
Gontcharov G. A., 2017, Astronomy Letters, 43, 472
Gullikson K., Kraus A., Dodson-Robinson S., 2016, AJ, 152, 40
Hall D. S., 1972, PASP, 84, 323
Handler G., Pigulski A., Daszyńska-Daszkiewicz J., Irrgang A., Kilkenny D., Guo A., Przybilla N., Alicavus F., Kallinger T., Pascual-Granado J., Niemczura E., Rozanski T., Chowdhury S., Buzasi D., Mirouh G., Simon-Diaz S., Moravveji E., De Cat P., 2019, ApJ, submitted
Holdsworth D. L., Smalley B., Gillon M., Clubb K. I., Southworth J., Maxted P. F. L., Anderson D. R., Barros S. C. C., Cameron A. C., Delrez L., Faedi F., Haswell C. A., Hellier C., Horne K., Jehin E., Norton A. J., Pollacco D., Skillen I., Smith A. M. S., West R. G., Wheatley P. J., 2014, MNRAS, 439, 2078
Jenkins J. M., Twicken J. D., McCauliff S., Campbell J., Sanderfer D., Lung D., Mansouri-Samani M., Girouard F., Tenenbaum P., Klaus T., Smith J. C., Caldwell D. A., Chacon A. D., Henze C., Heiges C., Latham D. W., Morgan E., Swade D., Rinehart S., Vanderspek R., 2016, in Proc. SPIE, Vol. 9913, Software and Cyberinfrastructure for Astronomy IV, p. 99133E
Kron G. E., 1947, PASP, 59, 261

Maeder A., Meynet G., 2004, A&A, 422, 225

Maehara H., Shibayama T., Notsu S., Notsu Y., Nagao T., Kusaba S., Honda S., Nogami D., Shibata K., 2012, Nature, 485, 478

Makarov V. V., 2003, AJ, 126, 1996

McQuillan A., Mazeh T., Aigrain S., 2013, ApJ, 775, L11

—, 2014, ApJS, 211, 24

Michaud G., 1970, ApJ, 160, 641

Miglio A., Montalbán J., Dupret M., 2007, Communications in Asteroseismology, 151, 48

Mowlavi N., Saesen S., Semaan T., Eggenberger P., Barblan F., Eyer L., Ekström S., Georgy C., 2016, A&A, 595, L1

Nielsen M. B., Gizon L., Schunker H., Karoff C., 2013, A&A, 557, L10

Paunzen E., Schnell A., Maitzen H. M., 2005, A&A, 444, 941

Pecaut M. J., Mamajek E. E., 2013, ApJS, 208, 9

Pedersen M. G., Antoci V., Korhonen H., White T. R., Jessen-Hansen J., Lehtinen J., Nikbakhsh S., Viuho J., 2017, MNRAS, 466, 3060

Pedersen M. G., Chowdhury S., Johnston C., Bowman D. M., Aerts C., Handler G., De Cat P., Neiner C., David-Uraz A., Buzasi D., Tkachenko a., Simon-Diaz S., Moravveji S., Sikora J., Mirouh G., Lovekin C., Cantiello M., Daszyńska-Daszkiewicz J., Pigulski A., 2019, ApJ, submitted

Ramiaramanantsoa T., Moffat A. F. J., Chené A.-N., Richardson N. D., Henrichs H. F., Desforges S., Antoci V., Rowe J. F., Matthews J. M., Kuschnig R., Weiss W. W., Sasselov D., Rucinski S. M., Guenther D. B., 2014, MNRAS, 441, 910

Ramiaramanantsoa T., Moffat A. F. J., Harmon R., Ignace R., St-Louis N., Vanbeveren D., Shenar T., Pablo H., Richardson N. D., Howarth I. D., Stevens I. R., Piaulet C., St-Jean L., Eversberg T., Pigulski A., Popowicz A., Kuschnig R., Zocłońska E., Buysschaert B., Handler G., Weiss W. W., Wade G. A., Rucinski S. M., Zwintz K., Luckas P., Heathcote B., Cacella P., Powles J., Locke M., Bohlsen T., Chené A.-N., Miszalski B., Waldron W. L., Kotze M. M., Kotze E. J., Böhm T., 2018, MNRAS, 473, 5532

Reinhold T., Reiners A., Basri G., 2013, A&A, 560, A4

Ricker G. R., Winn J. N., Vanderspek R., Latham D. W., Bakos G. Á., Bean J. L., Berta-Thompson Z. K., Brown T. M., Buchhave L., Butler N. R., Butler R. P., Chaplin W. J., Charbonneau D., Christensen-Dalsgaard J., Clampin M., Deming D., Doty J., De Lee N., Dressing C., Dunham E. W., Endl M., Fressin F., Ge J., Henning T., Holman M. J., Howard A. W., Ida S., Jenkins J. M., Jernigan G., Johnson J. A., Kaltenegger L., Kawai N., Kjeldsen H., Laughlin G., Levine A. M., Lin D., Lissauer J. J., MacQueen P., Marcy G., McCullough P. R., Morton T. D., Narita N., Paegert M., Palle E., Pepe F., Pepper J., Quirrenbach A., Rinehart S. A., Sasselov D., Sato B., Seager S., Sozzetti A., Stassun K. G., Sullivan P., Szentgyorgyi A., Torres G., Udry S., Villasenor J., 2015, Journal of Astronomical Telescopes, Instruments, and Systems, 1, 014003

Samus N. N., Durlevich O. V., et al., 2009, VizieR Online Data Catalog, 1, 2025

Scargle J. D., 1982, ApJ, 263, 835

Silaj J., Landstreet J. D., 2014, A&A, 566, A132

Soubiran C., Le Campion J.-F., Brouillet N., Chemin L., 2016, A&A, 591, A118

Spruit H. C., 1999, A&A, 349, 189

—, 2002, A&A, 381, 923

Stassun K. G., Oelkers R. J., Pepper J., Paegert M., De Lee N., Torres G., Latham D. W., Charpinet S., Dressing C. D., Huber D., Kane S. R., Lépine S., Mann A., Muirhead P. S., Rojas-Ayala B., Silvotti R., Fleming S. W., Levine A., Plavchan P., 2018, AJ, 156, 102

Strassmeier K. G., 2009, A&ARv, 17, 251

Urbaneja M. A., Kudritzki R.-P., Gieren W., Pietrzyński G., Bresolin F., Przybilla N., 2017, AJ, 154, 102

Wenger M., Ochsenbein F., Egret D., Dubois P., Bonnarel F., Borde S., Genova F., Jasniewicz G., Laloë S., Lesteven S., Monier R., 2000, A&AS, 143, 9